Compressive Angular and Frequency Periodogram Reconstruction for Multiband Signals

Dyonisius Dony Ariananda*, Daniel Romero†, and Geert Leus*
*Faculty of EEMCS, Delft University of Technology, The Netherlands
†Dept. of Signal Theory and Communications, University of Vigo, Spain
{d.a.dyonisius, g.j.t.leus}@tudelft.nl and dromero@gts.uvigo.es.

***Abstract*—In this paper, we present a duality between two problems: the reconstruction of the angular periodogram from spatial-domain signals received at different time indices and that of the frequency periodogram from time-domain signals received at different wireless sensors. We assume the existence of a multiband structure in either the angular or frequency domain representation of the received spatial or time-domain signal, respectively, where different bands are assumed to be uncorrelated. The two problems lead to a similar circulant structure in the so-called coset correlation matrix, which allows for a strong compression and a least-squares (LS) reconstruction approach. The LS reconstruction of the periodogram is possible under the full column rank condition of the system matrix, which is achievable by designing the spatial or temporal sampling patterns based on a circular sparse ruler.**

I. Introduction

The duality between the spectral analysis problems in the spatial-angular and time-frequency domains has been identified since decades. One application related to this duality is the direction of arrival (DOA) estimation and the frequency identification of sinusoids. In fact, this duality can be further exploited to handle different problems using the same algorithmic approach. In this paper, we underline a duality between the angular periodogram reconstruction from far-field signals received by an antenna array at different time indices (problem P1) and the frequency periodogram reconstruction by different wireless sensors based on the received time-domain signals (problem P2). We assume a multiband structure in either the angular or frequency domain representation of the received spatial or time-domain signal, respectively, where different bands are assumed to be uncorrelated. This uncorrelatedness emerges because the signals related to the different bands come from different users (more details later on) and it leads to a circulant structure in the so-called coset correlation matrix allowing for a strong compression, which is implemented using a periodic non-uniform linear array (non-ULA) in P1 and a multi-coset sampling in P2.

With respect to P1, our work is inspired by the work of [1], which focuses on the angular spectrum reconstruction from spatial-domain samples received by a non-ULA. However, the intention of [1] to reconstruct the actual angular spectrum instead of its periodogram leads to an underdetermined problem requiring a sparsity constraint on the angular domain to solve it. We will show in this paper that by focusing on only the angular periodogram reconstruction, we have an overdetermined problem that is solvable even without a sparsity constraint on the angular domain. This is useful for applications that need information only about the angular periodogram and not the actual angular spectrum. In the context of P2, some related works on compressive power spectrum estimation by a single sensor can be found in [2], [3]. The work of [2] attempts to reconstruct the unknown power spectrum of a wide-sense stationary signal from the obtained sub-Nyquist rate samples by exploiting the Toeplitz structure of the time-domain correlation matrix. The work of [3], which is related to our problem, considers the existence of a multiband signal where the spectra at different bands are uncorrelated. Hence, the correlation matrix of the entries at different bands has a diagonal structure. However, [3] does not focus on the strongest compression rate, relies on only one realization of the received signal, and uses frequency smoothing to approximate the correlation matrix computation. In contrast, we focus on the strongest compression rate, which can be obtained by exploiting the circulant structure of the coset correlation matrix and by solving the so-called minimal circular sparse ruler problem. In addition, in P2, we exploit the signals received by different sensors to approximate the correlation matrix computation.

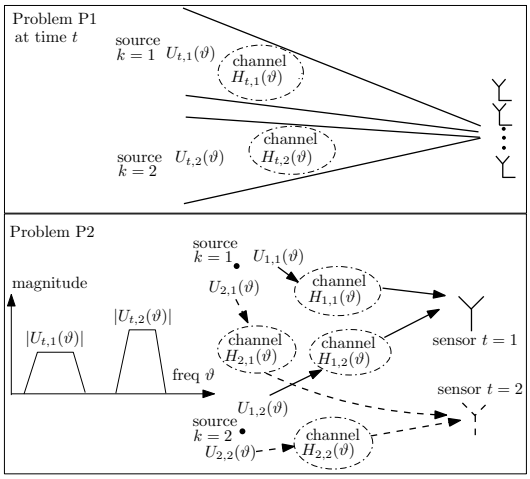

Fig. 1. The system model for problems P1 and P2.

II. System Model

We introduce the $\tilde{N} \times 1$ vector $\mathbf{x}_t = [x_t[0], x_t[1], \ldots, x_t[\tilde{N}-1]]^T$, where $x_t[\tilde{n}]$ represents the output of the $\tilde{n}$-th antenna in a ULA of $\tilde{N}$ antennas with half-wavelength spacing at time index t for P1 or the $\tilde{n}$-th sample out of $\tilde{N}$ consecutive Nyquist-rate samples received by the t-th sensor for P2. To obtain an accurate Fourier interpretation, we assume a relatively large $\tilde{N}$, which is easy to achieve for P2 and also true for P1 if we consider millimeter wave imaging applications where

*This work is supported in part by NWO-STW under the VICI program (project 10382). †D. Romero is supported by ERDF, TEC2010-21245-C02-02/TCM DYNACS, CONSOLIDERINGENIO 2010 CSD2008-00010 COMONSENS, FPU Grant AP2010-0149 and CN 2012/260 AtlantTIC.

the antenna spacing is very small and thus a large number of antennas is needed to cover the required aperture [1]. Denote the discrete-time Fourier transform (DTFT) of $x_t[\tilde{n}]$ by $X_t(\vartheta)$, which represents either the value of its angular spectrum at angle $\sin^{-1}(2\vartheta)$ with $\vartheta \in [-0.5, 0.5)$ or that of its frequency spectrum at frequency ϑ. Since $X_t(\vartheta)$ at $\vartheta \in [0.5, 1)$ is a replica of $X_t(\vartheta)$ at $\vartheta \in [-0.5, 0)$, we focus on $X_t(\vartheta)$ in $\vartheta \in [0, 1)$ to simplify the discussion. We consider K active bands in the ϑ-domain, denote the support of the k-th active band by $\mathcal{B}_k$, and define the bandwidth of the k-th active band as $\Lambda(\mathcal{B}_k) = \sup\{\mathcal{B}_k\} - \inf\{\mathcal{B}_k\}$. We assume that $\max_k \Lambda(\mathcal{B}_k)$ is known, which is reasonable, especially for P2, as the channelization parameter for a communication network is usually known.

Let us split the $\tilde{N}$ uniform grid points (which are the antennas in the ULA for P1 or the indices of the Nyquist-rate samples for P2) into L non-overlapping blocks of N uniform grid points. Collect all the $(n+1)$-th grid points from each of the L blocks and call this collection of grid points, i.e., $\{\tilde{n} | \tilde{n} \in \{0, 1, \ldots, \tilde{N}-1\}, \tilde{n} \bmod N = n\}$, the $(n+1)$-*th coset*. For clarity of the discussion, the *coset index* of the $(n+1)$-th coset is n. In this way, we can view the earlier uniform sampling as a multi-coset sampling [4] with N cosets. For P1, this is equivalent to perceiving the ULA of $\tilde{N}$ antennas as N interleaved uniform linear subarrays (ULSs) [1] (which are the cosets), each of which has L antennas with spacing $N\lambda/2$ where λ is the wavelength. For P2, we can perceive the $\tilde{N}$ time-domain samples in $\mathbf{x}_t$ as the output of a time-domain multi-coset sampler with L samples per coset. When only the $(n+1)$-th coset is active, we obtain

$$x_{t,n}[\tilde{n}] = x_t[\tilde{n}] \sum_{l=0}^{L-1} \delta[\tilde{n} - (lN + n)], \quad 0 \le n \le N-1, \quad (1)$$

which can be stacked into the $\tilde{N} \times 1$ vector $\mathbf{x}_{t,n} = [x_{t,n}[0], x_{t,n}[1], \ldots, x_{t,n}[\tilde{N}-1]]^T$. Note that $\mathbf{x}_t = \sum_{n=0}^{N-1} \mathbf{x}_{t,n}$. By splitting $\vartheta \in [0, 1)$, without loss of generality, into N equal-width bins and writing the spectrum at the $(i+1)$-th bin ($0 \le i \le N-1$) as $X_t^{(i)}(\vartheta) = X_t\left(\vartheta + \frac{i}{N}\right)$ with ϑ now limited to $\vartheta \in [0, 1/N)$, the DTFT of $x_{t,n}[\tilde{n}]$ for $0 \le n \le N-1$ is found as [4]

$$X_{t,n}(\vartheta) = \frac{1}{N} \sum_{i=0}^{N-1} X_t^{(i)}(\vartheta) e^{\frac{j2\pi ni}{N}}, \quad \vartheta \in [0, 1/N). \quad (2)$$

It is clear from (2) that the spectrum $X_{t,n}(\vartheta)$ at each ϑ is a sum of the N aliases of $X_t(\vartheta)$ at N different bins since either the spatial or temporal sampling rate becomes $1/N$ times the Nyquist rate. Stacking $\{X_{t,n}(\vartheta)\}_{n=0}^{N-1}$ in (2) into an $N \times 1$ vector $\bar{\mathbf{x}}_t(\vartheta) = [X_{t,0}(\vartheta), X_{t,1}(\vartheta), \ldots, X_{t,N-1}(\vartheta)]^T$ leads to

$$\bar{\mathbf{x}}_t(\vartheta) = \mathbf{B}\mathbf{x}_t(\vartheta), \quad \vartheta \in [0, 1/N), \quad (3)$$

where $\mathbf{x}_t(\vartheta) = [X_t^{(0)}(\vartheta), X_t^{(1)}(\vartheta), \ldots, X_t^{(N-1)}(\vartheta)]^T$ is the $N \times 1$ vector and the element of the $N \times N$ matrix $\mathbf{B}$ at the $(n+1)$-th row and the $(i+1)$-th column is given by $[\mathbf{B}]_{n+1,i+1} = \frac{1}{N} e^{\frac{j2\pi ni}{N}}$.

At this stage, let us consider the model in Fig. 1, assume that the K active bands correspond to K different users, and introduce $U_{t,k}(\vartheta)$ and $H_{t,k}(\vartheta)$ as:

- $U_{t,k}(\vartheta)$ is the source signal related to the k-th user received at time index t (for P1) or at sensor t (for P2). For P1 it can vary with the DOA $\sin^{-1}(2\vartheta)$ within the k-th band due to scattering, whereas for P2 it can vary with frequency ϑ within the k-th band due to power loading.
- $H_{t,k}(\vartheta)$ is the related channel response for the k-th user at time index t and DOA $\sin^{-1}(2\vartheta)$ (for P1) or at sensor t and frequency ϑ (for P2).

Based on those definitions, for the noiseless case, we can write

$$X_t^{(i)}(\vartheta) = \sum_{k=1}^{K} H_{t,k}^{(i)}(\vartheta) U_{t,k}^{(i)}(\vartheta), \ \vartheta \in [0, 1/N), \quad (4)$$

with $H_{t,k}^{(i)}(\vartheta) = H_{t,k}\left(\vartheta + \frac{i}{N}\right)$ and $U_{t,k}^{(i)}(\vartheta) = U_{t,k}\left(\vartheta + \frac{i}{N}\right)$. In general, we may assume that $X_t^{(i)}(\vartheta)$ varies with t because either one (or both) of the following situations occurs

- For P1, the k-th user's source signal $U_{t,k}(\vartheta)$ varies with the time index t due to the fact that the information that is being transmitted changes with time. For P2, it varies with the sensor index t where the signal is received due to the fact that sensors are not synchronized.
- For P1, the k-th user's channel response $H_{t,k}(\vartheta)$ varies with the time index t due to Doppler fading effects. For P2, it varies with the sensor index t where the signal is received, due to path loss, shadowing, and small-scale spatial fading effects.

As a result, we can compute the expectations over t that will follow later on in this paper by considering different realizations of $X_t^{(i)}(\vartheta)$ in t and by simple averaging. We will come back to this issue later on.

Since the K different active bands in $X_t(\vartheta)$ correspond to K different users which in general transmit mutually uncorrelated source signals, we can assume that these K bands are also mutually uncorrelated. For both problems, this assumption is even enforced since the signals from different users pass through mutually uncorrelated wireless channels on their way to the receiver, as long as the bands (in angle for P1 or in frequency for P2) and/or the frequencies (for P1) or the locations (for P2) of the different users (source signals) are sufficiently separated (sufficient in the sense that no coherence is observed). Now, observing that N is a design parameter related to the width of the predefined bins in $\vartheta \in [0, 1)$, and setting its value according to $\frac{1}{N} \ge \max_k \Lambda(\mathcal{B}_k)$, we can find that for each $\vartheta \in [0, 1/N)$, every active band in $X_t(\vartheta)$ has a contribution in at most one entry $X_t^{(i)}(\vartheta)$ of $\mathbf{x}_t(\vartheta)$ in (3). Taking also the above uncorrelatedness assumption into account, it is clear that the $N \times N$ correlation matrix $\mathbf{R}_x(\vartheta) = E_t[\mathbf{x}_t(\vartheta)\mathbf{x}_t^H(\vartheta)]$ is a diagonal matrix for all $\vartheta \in [0, 1/N)$. We then define the so-called $N \times N$ coset correlation matrix as $\mathbf{R}_{\bar{x}}(\vartheta) = E_t[\bar{\mathbf{x}}_t(\vartheta)\bar{\mathbf{x}}_t^H(\vartheta)]$, which can be written as

$$\mathbf{R}_{\bar{x}}(\vartheta) = \mathbf{B}\mathbf{R}_x(\vartheta)\mathbf{B}^H, \quad \vartheta \in [0, 1/N). \quad (5)$$

Since $\mathbf{R}_x(\vartheta)$ is a diagonal matrix and it is clear from (3) that $\mathbf{B}$ is an inverse discrete Fourier transform (IDFT) matrix, it is then obvious that $\mathbf{R}_{\bar{x}}(\vartheta)$ is a circulant matrix.

III. Spatial or Temporal Compression

In this section, we intend to exploit the circulant structure of $\mathbf{R}_{\bar{x}}(\vartheta)$ in (5), which generally contains redundant informa-

tion, allowing us to perform either spatial or temporal compression. Due to its circularity, we can condense $\mathbf{R}_{\bar{x}}(\vartheta)$ into an $N \times 1$ vector $\mathbf{r}_{\bar{x}}(\vartheta) = [r_{\bar{x}}(\vartheta, 0), r_{\bar{x}}(\vartheta, 1), \ldots, r_{\bar{x}}(\vartheta, N-1)]^T$ and write

$$\text{vec}(\mathbf{R}_{\bar{x}}(\vartheta)) = \bar{\mathbf{T}}\mathbf{r}_{\bar{x}}(\vartheta), \quad \vartheta \in [0, 1/N), \tag{6}$$

where $r_{\bar{x}}(\vartheta, (n-n') \bmod N) = E_t\left[X_{t,n}(\vartheta), X^*_{t,n'}(\vartheta)\right]$ with $s \bmod N$ the remainder of the integer division s/N, vec(.) is the operator that stacks all columns of a matrix into one column vector and $\bar{\mathbf{T}}$ is an $N^2 \times N$ repetition matrix whose j-th row is given by the $\left(\left(j-1-\left\lfloor\frac{j-1}{N}\right\rfloor\right) \bmod N+1\right)$-th row of the $N \times N$ identity matrix $\mathbf{I}_N$. Since the N^2 elements of $\mathbf{R}_{\bar{x}}(\vartheta)$ can be condensed into the N elements of $\mathbf{r}_{\bar{x}}(\vartheta)$, we introduce a compression (similar to [4]) by activating only $M < N$ cosets leading to a classical non-uniform periodic sampling in either the spatial or time domain, where the indices of the M active cosets are given by the set $\mathcal{M} = \{n_0, n_1, \ldots, n_{M-1}\}$ with $0 \leq n_0 \leq n_1 \leq \cdots \leq n_{M-1} \leq N-1$. Here, we collect all values of $x_{t,n}[\tilde{n}]$ in (1) and compute their corresponding DTFT $X_{t,n}(\vartheta)$ in (2) for all $n \in \mathcal{M}$. We then stack $\{X_{t,n}(\vartheta)\}_{n\in\mathcal{M}}$ into an $M \times 1$ vector $\bar{\mathbf{y}}_t(\vartheta)$ as $\bar{\mathbf{y}}_t(\vartheta) = [X_{t,n_0}(\vartheta), X_{t,n_1}(\vartheta), \ldots, X_{t,n_{M-1}}(\vartheta)]^T$ and relate $\bar{\mathbf{y}}_t(\vartheta)$ to $\bar{\mathbf{x}}_t(\vartheta)$ in (3) as

$$\bar{\mathbf{y}}_t(\vartheta) = \bar{\mathbf{C}}_{\mathcal{M}}\bar{\mathbf{x}}_t(\vartheta), \quad \vartheta \in [0, 1/N),$$

where $\bar{\mathbf{C}}_{\mathcal{M}}$ is an $M \times N$ selection matrix whose rows are selected from the rows of $\mathbf{I}_N$ according to $\mathcal{M}$. Hence, we can compute the correlation matrix of $\bar{\mathbf{y}}_t(\vartheta)$ for $\vartheta \in [0, 1/N)$ as

$$\mathbf{R}_{\bar{y}}(\vartheta) = E_t[\bar{\mathbf{y}}_t(\vartheta)\bar{\mathbf{y}}^H_t(\vartheta)] = \bar{\mathbf{C}}_{\mathcal{M}}\mathbf{R}_{\bar{x}}(\vartheta)\bar{\mathbf{C}}^H_{\mathcal{M}}. \tag{7}$$

Stacking all columns of $\mathbf{R}_{\bar{y}}(\vartheta)$ into a column vector $\text{vec}(\mathbf{R}_{\bar{y}}(\vartheta))$ as well as considering (6) and the realness of $\bar{\mathbf{C}}_{\mathcal{M}}$, we have

$$\text{vec}(\mathbf{R}_{\bar{y}}(\vartheta)) = \mathbf{R}_{\bar{C}_{\mathcal{M}}}\mathbf{r}_{\bar{x}}(\vartheta), \quad \vartheta \in [0, 1/N), \tag{8}$$

where $\mathbf{R}_{\bar{C}_{\mathcal{M}}} = (\bar{\mathbf{C}}_{\mathcal{M}} \otimes \bar{\mathbf{C}}_{\mathcal{M}})\bar{\mathbf{T}}$ is an $M^2 \times N$ matrix and $\otimes$ represents the Kronecker product operation.

In practice, we approximate the expectation operation in (7) by taking an average over the signals at different time indices t for P1 or at different sensors t for P2, i.e., we estimate $\mathbf{R}_{\bar{y}}(\vartheta)$ as $\hat{\mathbf{R}}_{\bar{y}}(\vartheta) = \frac{1}{\tau}\sum_{t=1}^{\tau}\bar{\mathbf{y}}_t(\vartheta)\bar{\mathbf{y}}^H_t(\vartheta)$, which can be written as

$$\hat{\mathbf{R}}_{\bar{y}}(\vartheta) = \bar{\mathbf{C}}_{\mathcal{M}}\hat{\mathbf{R}}_{\bar{x}}(\vartheta)\bar{\mathbf{C}}^H_{\mathcal{M}} = \bar{\mathbf{C}}_{\mathcal{M}}\mathbf{B}\hat{\mathbf{R}}_x(\vartheta)\mathbf{B}^H\bar{\mathbf{C}}^H_{\mathcal{M}}, \tag{9}$$

for all $\vartheta \in [0, 1/N)$, where τ represents either the total number of time indices or sensors used in the averaging process and where $\hat{\mathbf{R}}_x(\vartheta) = \frac{1}{\tau}\sum_{t=1}^{\tau}\mathbf{x}_t(\vartheta)\mathbf{x}^H_t(\vartheta)$ is generally not a diagonal matrix for a finite τ. Note that, for both problems, this requires either $H^{(i)}_{t,k}(\vartheta)$ or $U^{(i)}_{t,k}(\vartheta)$ in (4) or both of them to have different values for different indices t (as discussed earlier). Also observe that as τ is getting very large, $\hat{\mathbf{R}}_x(\vartheta)$ and the estimated coset correlation matrix $\hat{\mathbf{R}}_{\bar{x}}(\vartheta)$ will be asymptotically diagonal and circulant, respectively.

IV. Reconstruction

Observe that it is possible to have a tall matrix $\mathbf{R}_{\bar{C}_{\mathcal{M}}}$ in (8) since we can have $M^2 \geq N$ despite $M < N$. Hence, it is also possible to reconstruct $\mathbf{r}_{\bar{x}}(\vartheta)$ in (8) from $\text{vec}(\mathbf{R}_{\bar{y}}(\vartheta))$ using least-squares (LS) for all $\vartheta \in [0, 1/N)$ as long as $\mathbf{R}_{\bar{C}_{\mathcal{M}}}$ has full column rank. Note that estimators other than LS could be considered as long as the identifiability of $\mathbf{r}_{\bar{x}}(\vartheta)$ in (8) is preserved [8]. As it is clear that each row of both $\bar{\mathbf{C}}_{\mathcal{M}} \otimes \bar{\mathbf{C}}_{\mathcal{M}}$ and $\bar{\mathbf{T}}$ in (8) has exactly a single one at one entry and zeros elsewhere, every row of $\mathbf{R}_{\bar{C}_{\mathcal{M}}}$ also has a single one at a certain entry and zeros elsewhere. Hence, $\mathbf{R}_{\bar{C}_{\mathcal{M}}}$ will have full column rank if each of its columns has at least a single one. Denoting the f-th row of $\mathbf{I}_N$ as $\mathbf{e}^T_f$, we have the following lemma.

Lemma 1: If $f-1, g-1 \in \mathcal{M}$, i.e., $\mathbf{e}^T_f$ and $\mathbf{e}^T_g$ are two rows of $\bar{\mathbf{C}}_{\mathcal{M}}$, then at least two rows of $\mathbf{R}_{\bar{C}_{\mathcal{M}}}$ are given by the $((g-f) \bmod N+1)$-th and the $((f-g) \bmod N+1)$-th rows of $\mathbf{I}_N$.

Proof: The fact that each row of $\bar{\mathbf{C}}_{\mathcal{M}} \otimes \bar{\mathbf{C}}_{\mathcal{M}}$ only contains a one at one entry and zeros elsewhere means that each row of $\mathbf{R}_{\bar{C}_{\mathcal{M}}}$ is generated by selecting one of the rows of $\bar{\mathbf{T}}$. For example, if the j-th row of $\bar{\mathbf{C}}_{\mathcal{M}} \otimes \bar{\mathbf{C}}_{\mathcal{M}}$ has a one at the j'-th entry, the j-th row of $\mathbf{R}_{\bar{C}_{\mathcal{M}}}$ is equal to the j'-th row of $\bar{\mathbf{T}}$. Since $\mathbf{e}^T_f \otimes \mathbf{e}^T_g$ has a one at the $(N(f-1)+g)$-th entry and zeros elsewhere, it is clear that the existence of $\mathbf{e}^T_f$ and $\mathbf{e}^T_g$ in $\bar{\mathbf{C}}_{\mathcal{M}}$ ensures that $\mathbf{R}_{\bar{C}_{\mathcal{M}}}$ has the $(N(f-1)+g)$-th and $(N(g-1)+f)$-th rows of $\bar{\mathbf{T}}$ as two of its rows. By recalling that the j-th row of $\bar{\mathbf{T}}$ is given by the $\left(\left(j-1-\left\lfloor\frac{j-1}{N}\right\rfloor\right) \bmod N+1\right)$-th row of $\mathbf{I}_N$, we can find that the $(N(f-1)+g)$-th and the $(N(g-1)+f)$-th rows of $\bar{\mathbf{T}}$ are given by the $((g-f) \bmod N+1)$-th and the $((f-g) \bmod N+1)$-th rows of $\mathbf{I}_N$, respectively. This concludes the proof. □

Let us now review the concept of a circular sparse ruler defined in [5]. Using this concept and Lemma 1, Theorem 1 then directly follows.

Definition 1: A circular sparse ruler of length $N-1$ is defined as a set $\mathcal{P} \subset \{0, 1, \ldots, N-1\}$ such that $\{(p-p') \bmod N | \forall p, p' \in \mathcal{P}\} = \{0, 1, \ldots, N-1\}$. It is called minimal if no other circular sparse ruler of length $N-1$ exists with less elements.

Theorem 1: Defining Ω as $\Omega = \{(g-f) \bmod N | \forall f-1, g-1 \in \mathcal{M}\}$, the full column rank condition of $\mathbf{R}_{\bar{C}_{\mathcal{M}}}$ is ensured if $\Omega = \{0, 1, \ldots, N-1\}$. In other words, $\mathbf{R}_{\bar{C}_{\mathcal{M}}}$ will have full column rank if it has all rows of $\mathbf{I}_N$ as its rows. In this case, the set $\mathcal{M}$ is equivalent to a circular sparse ruler of length $N-1$.

The readers are referred to [5] in order to obtain more detailed information about circular as well as linear sparse rulers. Given the set Ω, we now aim to obtain the best possible compression rate M/N by minimizing $|\mathcal{M}| = M$, which is the cardinality of $\mathcal{M}$ or the number of marks in the length-$(N-1)$ circular sparse ruler. As a result, we can write our problem as

$$\min_{\mathcal{M}} |\mathcal{M}| \text{ s.t. } \Omega = \{0, 1, \ldots, N-1\}. \tag{10}$$

The problem in (10) boils down to a length-$(N-1)$ minimal circular sparse ruler problem. Solving this problem basically minimizes the compression rate M/N while maintaining the uniqueness of the LS solution for the problems in (8).

We now make some notes with respect to P1. Configuring a linear array geometry based on a solution of the minimal linear sparse ruler problem generally leads to the famous minimum redundancy array (MRA) [6], whose geometry can be used to form a virtual array (called co-array) that is uniform. This is useful in DOA estimation as it is possible to apply spatial smoothing followed by MUSIC [7]. However, our problem here does not need the existence of a uniform co-array. Hence, we use our ULA as the *underlying* array and activate only

$M < N$ ULSs in this ULA with the indices of the active ULSs given by $\mathcal{M}$ leading to a periodic non-ULA of active antennas with the location of the active antennas in each spatial period governed by $\mathcal{M}$. If $\mathcal{M}$ is a solution of the minimal length-$(N-1)$ circular sparse ruler problem in (10), we label one spatial period of the resulting non-ULA of active antennas as a *circular MRA* and the entire array of active antennas as a *periodic circular MRA*. Similarly for P2, if the indices of the $M < N$ active cosets in the temporal sampling are given by the solution of (10), then we can label the non-uniform sampling in one temporal period as *minimal circular sparse ruler sampling* and the periodic non-uniform sampling as *periodic minimal circular sparse ruler sampling*.

After the LS reconstruction of $\mathbf{r}_{\bar{x}}(\vartheta)$ in (8) from $\text{vec}(\mathbf{R}_{\bar{y}}(\vartheta))$ for $\vartheta \in [0, 1/N)$ given the full column rank condition of $\mathbf{R}_{\bar{C}_{\mathcal{M}}}$, we can compute $\mathbf{R}_{\bar{x}}(\vartheta)$ from $\mathbf{r}_{\bar{x}}(\vartheta)$ using (6), and $\mathbf{R}_x(\vartheta)$ from $\mathbf{R}_{\bar{x}}(\vartheta)$ using (5) as $\mathbf{R}_x(\vartheta) = N^2\mathbf{B}^H\mathbf{R}_{\bar{x}}(\vartheta)\mathbf{B}$. Recall that $\text{diag}(\mathbf{R}_x(\vartheta)) = [E_t[|X_t^{(0)}(\vartheta)|^2], E_t[|X_t^{(1)}(\vartheta)|^2], \ldots, E_t[|X_t^{(N-1)}(\vartheta)|^2]]^T$ with $\vartheta \in [0, 1/N)$. Reconstructing $\text{diag}(\mathbf{R}_x(\vartheta))$ for $\vartheta \in [0, 1/N)$ will thus give $E_t[|X_t(\vartheta)|^2]$ for all $\vartheta \in [0, 1)$. In practice however, we only have $\frac{1}{\tau}\sum_{t=1}^{\tau}|X_t(\vartheta)|^2$ for all $\vartheta \in [0, 1)$, which is available as the diagonal elements of $\hat{\mathbf{R}}_x(\vartheta)$ in (9). In this case, $\frac{1}{\tilde{N}\tau}\sum_{t=1}^{\tau}|X_t(\vartheta)|^2$ for all $\vartheta \in [0, 1)$ can be considered as the averaged periodogram of the signals received at different times t in P1 or at different sensors t in P2.

TABLE I. THE FREQUENCY BANDS OCCUPIED BY THE USERS, THEIR NORMALIZED MAGNITUDE, AND THE EXPERIENCED PATH LOSS

User band (ϑ)	Normalized magnitude/freq. (per rad/sample)	Path loss at each sensor
$[\frac{-8}{18}, \frac{-7}{18}]$	32 dBm (1.585 W)	-13 dB (0.0501)
$[\frac{-6}{18}, \frac{-5}{18}]$	35 dBm (3.162 W)	-19 dB (0.0126)
$[\frac{-5}{18}, \frac{-4}{18}]$	38 dBm (6.31 W)	-18 dB (0.0158)
$[\frac{-3}{18}, \frac{-2}{18}]$	40 dBm (10 W)	-19 dB (0.0126)
$[\frac{1}{18}, \frac{2}{18}]$	34 dBm (2.512 W)	-11 dB (0.0794)
$[\frac{3}{18}, \frac{4}{18}]$	34 dBm (2.512 W)	-17 dB (0.0200)

V. NUMERICAL STUDY

In this section, we evaluate our approach by focusing only on P2. However, the result of the numerical study is also applicable to P1 since both problems are dual. Here, we have $\tilde{N} = 306$, $L = 17$ and $N = 18$ where $\tilde{N}$ indicates the number of available time-domain samples in each sensor if the received signal is sampled at Nyquist rate. However, every sensor employs periodic circular sparse ruler sampling by collecting only $M = 5$ out of $N = 18$ possible samples based on $\mathcal{M} = \{0, 1, 4, 7, 9\}$ obtained by solving the length-17 minimal circular sparse ruler problem. This is equivalent to constructing a 5×18 matrix $\bar{\mathbf{C}}_{\mathcal{M}}$ in (7) whose rows are selected from the rows of $\mathbf{I}_{18}$ based on $\mathcal{M}$ leading to a compression rate of $M/N = 0.278$. This choice of $\bar{\mathbf{C}}_{\mathcal{M}}$ ensures the full column rank condition of $\mathbf{R}_{\bar{C}_{\mathcal{M}}}$ in (8). We consider $\tau = 200$ fully synchronized sensors that observe one realization of six user signals, i.e., $U_{t,k}(\vartheta) = U_k(\vartheta)$, whose frequency components are indicated in Table I together with the magnitude $|U_k(\vartheta)|^2$ at each band normalized by $\tilde{N}$. At each sensor, we assume the existence of temporal white noise with variance $\sigma_n^2 = 7$ dBm. In general, the signal of each user received by different sensors passes through different wireless channels $H_{t,k}(\vartheta)$. However, to simplify the simulation study, the signal from a certain user received by all sensors is assumed to experience the same path loss and shadowing. We indicate the amount of path loss experienced between a particular user and all sensors in Table I. Here, this path loss value is assumed to include the shadowing effect to simplify the simulation. On top of the path loss, the existence of small-scale Rayleigh fading is simulated by generating the channel frequency response $H_{t,k}(\vartheta)$ according to a zero-mean complex Gaussian distribution with variance governed by the amount of path loss in Table I. The fading experienced by each band is assumed to be flat. Fig. 2 illustrates the computed periodogram of the user signals as a function of frequency scaled by the fading averaged across all sensors. Here, the Nyquist-rate based estimate (obtained by collecting all $\tilde{N}$ samples) is provided as a reference. The figure indicates that, with respect to the Nyquist-rate based estimate, the quality of the reconstructed periodogram of the faded user signals is still acceptable despite a very strong compression. For the purpose of spectrum sensing (such as in cognitive radio networks), this approach could be interesting since the six active bands can still be correctly located despite the degradation in the estimation quality and a significant leakage introduced by the strong compression in the unoccupied bands. Note that estimators other than LS can be considered and they might lead to a better performance [8].

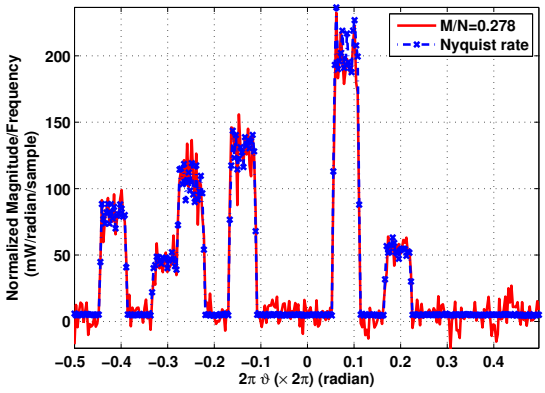

Fig. 2. The reconstructed periodogram of the faded user signals as a function of frequency.

REFERENCES

[1] J.D. Krieger, Y. Kochman, and G.W. Wornell, "Design and analysis of multi-coset arrays," *Proc. IEEE International Conference on Acoustics, Speech and Signal Processing*, Vancouver, pp. 3781-3785, May 2013.

[2] D.D. Arianandа and G. Leus, "Compressive wideband power spectrum estimation," *IEEE Transactions on Signal Processing*, vol. 60, no. 9, pp. 4775-4789, September 2012.

[3] C.P. Yen, Y. Tsai, and X. Wang, "Wideband Spectrum Sensing Based on Sub-Nyquist Sampling," *IEEE Transactions on Signal Processing*, vol. 61, no. 12, pp. 3028-3040, June 2013.

[4] M. Mishali and Y. Eldar, "Blind multiband signal reconstruction: compressed sensing for analog signals," *IEEE Transactions on Signal Processing*, vol. 57, no. 3, pp. 993-1009, March 2009.

[5] D. Romero and G. Leus, "Compressive covariance sampling," *Proc. Inf. Theory Appl. Workshop (ITA 2013)*, San Diego, California, Feb. 2013.

[6] A. Moffet, "Minimum-redundancy linear arrays," *IEEE Trans. Antennas Propag.*, vol. 16, no. 2, pp. 172-175, Mar. 1968.

[7] S. Shakeri, D.D. Arianandа, and G. Leus, "Direction of arrival estimation using sparse ruler array design," *Proc. IEEE Workshop on Signal Process. Adv. Wireless Commun.*, Cesme, pp. 525-529, June 2012.

[8] D. Romero and G. Leus, "Wideband spectrum sensing from compressed measurements using spectral prior information," *IEEE Transactions on Signal Processing*, to appear.